On the Expandability of Free-Space Micromachined Optical Cross Connects

Lih-Yuan Lin, *Member, IEEE, Member, OSA*, Evan L. Goldstein, *Member, IEEE*, and Robert W. Tkach, *Senior Member, IEEE, Fellow, OSA*

***Abstract*—Free-space micromachined optical-switching technology has emerged as a promising candidate for the large-scale optical cross connects that are needed in next-generation optical-transport networks. Although this technology has demonstrated good optical performance, its ability to expand to the required port-count while remaining within reasonable optical loss budgets has yet to be demonstrated. In this paper, we theoretically analyze the expandability of free-space micromachined optical switches. The chief loss mechanisms—Gaussian-beam divergence and angular misalignment—are analyzed both theoretically and experimentally. We find that micromirror angular repeatability in such a cross connect must be accurate within about 0.1°, and show that integrated mechanical structures are capable of achieving this goal. These results in general suggest that free-space micromachined optical-switching technology appears capable of achieving the port-count required by core-transport networks while remaining within cross-office optical-loss budgets.**

***Index Terms*—Free-space, micromachines, micromirrors, optical coupling, optical cross connects, optical switching.**

I. Introduction

As THE channel-count and bit-rate in wavelength-division-multiplexed (WDM) transport systems has lurched upward, and the demand for data-networking capacity has grown, it becomes increasingly desirable to manage optical networks at the wavelength level (OC-48 and beyond). Optical-layer cross connects (OXC's) with high port-count—on the order of 1000—are emerging as the chief candidates for achieving this.

This vision imposes stringent requirements on the OXC's, however, chiefly in the areas of port-count and loss budget. Indeed, no optical technologies have yet demonstrated that they can meet these challenges, leaving the field, at least in the interim, to electronic switch fabrics. Recently, however, free-space optical MEMS (micro-electro-mechanical systems) technologies have begun to show promise for this application. This is in large part due to the technology's unique feature of combining the merits of free-space optics and integrated photonics. Moreover, the MEMS fabrication process allows integration of optical, electrical, and mechanical structures on a single chip, thus greatly enhancing the functionality of MEMS–based OXC's.

Manuscript received July 2, 1999; revised November 29, 1999.

L.-Y. Lin and E. L. Goldstein were with AT&T Labs-Research, Red Bank, NJ 07701 USA. They are now with Tellium, Inc., Oceanport, NJ 07757 USA (e-mail: lylin@tellium.com).

R. W. Tkach is with AT&T Labs-Research, Red Bank, NJ 07701 USA.

Publisher Item Identifier S 0733-8724(00)03038-3.

Free-space MEMS-based optical switches have been demonstrated in 2×2 form [1], [2] and in slightly larger $M \times N$ prototypes [3]–[7]. These accomplishments have rapidly revealed the intrinsically good optical quality of free-space interconnects, particularly in the areas of crosstalk, polarization, and wavelength-independence, and bit-rate transparency. The demonstrated switching times are also well suited for the applications of OXC's. However, the issue of tight optical-alignment tolerances in free-space optics remains to be solved. In particular, the divergence of optical beams with increasing propagation distance, the angular misalignment of the optical beam with respect to the receiving fibers, and the quality of the micromirrors, all affect the expandability of free-space MEMS OXC's in ways that have not been systematically addressed.

In this paper, we present a theoretical analysis of the effect of optical-beam divergence and angular misalignment on the expandability of free-space OXC's. The analysis is based on general Gaussian-beam theory, and is therefore independent of the underlying technologies used either for the switch fabrics or for fiber packaging. Experimental measurements have also been performed to support the theoretical analysis. These will be covered in Section II (Gaussian-beam divergence) and Section III (angular dependence). In the free-space MEMS optical switches that we have demonstrated, free-rotating hinged micromirrors are utilized as the switching elements [4]. This approach eliminates the potential problem of long-term material memory and fatigue when mirror actuation angle exceeds the material limitation [8], both of which are significant issues in OXC's used as facilities switches, with configuration-holding-times that may be measured in years. One pays for this advantage of free-rotating hinge structures, however, in the form of decreased angular precision. Here again, however, the integrated manufacture of MEMS structures comes to the rescue. We demonstrate enhanced mechanical designs for the free-rotating hinges and micro-actuators that achieve better than 0.1° angular precision. The results are described in Section III. In Section IV, we present means of improving mirror flatness and show that it is feasible to achieve nearly flat micromirrors exhibiting high-optical quality.

II. Effects of Gaussian-Beam Divergence

A general representation of a matrix-type $M \times N$ free-space MEMS optical switch is shown in Fig. 1. Such a switch utilizes reflection from switch mirrors that are rotated up to redirect input optical beams to the desired output fibers. Fig. 2 shows a scanning-electron micrograph (SEM) of an 8×8 switch with free-rotating micromirrors that we have demonstrated. The device was fabricated at Cronos Integrated Microsystems using

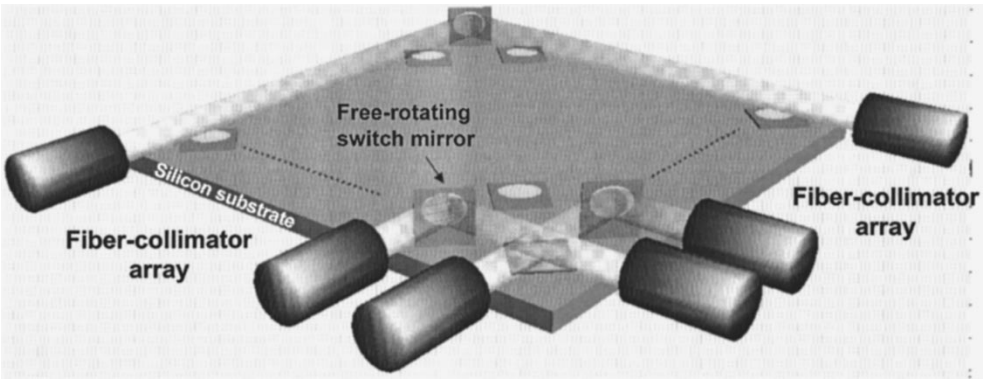

Fig. 1. Schematic drawing of a free-space MEMS optical switch.

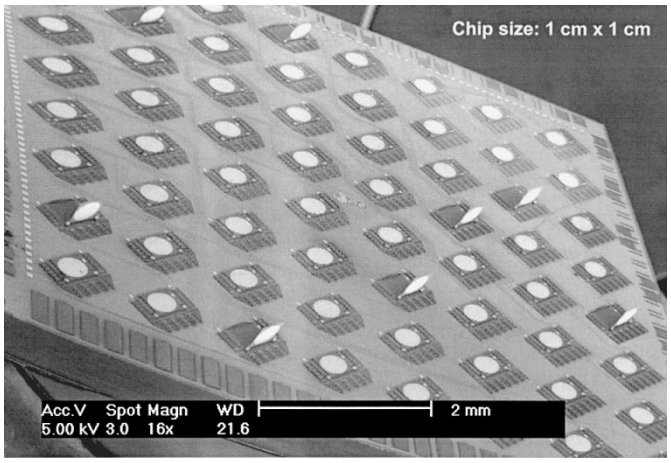

Fig. 2. Scanning electron micrograph (SEM) of an 8×8 MEMS optical switch.

the MUMPS process [9]. The collimated optical beams diverge as they propagate through free space due to the finite emitting beam aperture. This imposes fundamental limits on optical coupling efficiency. We evaluate these limits using general Gaussian-beam theory [10], so our analysis is independent of the means used to produce the collimated beams (e.g., fibers with attached GRIN lenses, or single-mode fibers with microlenses), as well as the switch fabric geometries.

To begin, we define the system's "emitting plane" and "receiving plane" as the planes in which the optical beams are emitted and received, respectively. The lowest-order mode ($\text{TEM}_{0,0}$) of a Gaussian-beam can be expressed as [10]

$$\begin{aligned} E(x,y,z) &= E_0\left\{\frac{w_0}{w(z)}\exp\left[-\frac{r^2}{w^2(z)}\right]\right\} \text{ amplitude factor} \\ &\quad\times\exp\left\{-j\left[kz-\tan^{-1}\left(\frac{z}{z_0}\right)\right]\right\} \text{ longitudinal factor} \\ &\quad\times\exp\left[-j\frac{kr^2}{2R(z)}\right] \text{ radial phase} \end{aligned} \tag{1}$$

where

z propagation direction of the Gaussian-beam;

$r=\sqrt{x^2+y^2}$ distance from the axis of the Gaussian-beam;

k $2\pi/\lambda$;

w_0 $1/e$ half-width at beam-waist.

z_0 is a parameter defined as

$$z_0=\frac{\pi w_0^2}{\lambda} \tag{2}$$

for free space. The divergence of the optical beam results in an increase of the $1/e$ half-width $w(z)$ with z given by

$$w(z)=w_0\sqrt{1+\left(\frac{z}{z_0}\right)^2} \tag{3}$$

and yields a curved wave-front whose radius is represented by

$$R(z)=z\left[1+\left(\frac{z_0}{z}\right)^2\right]. \tag{4}$$

The coupling efficiency Γ can be obtained by computing the normalized overlap integral of the divergent Gaussian-beam wave function at the receiver plane and the modal wave function of the receiving optics. Here, we restrict ourselves to the situation of chief interest, in which both the emitting optics and the receiving optics are identical, with only fundamental propagating modes. Without angular misalignment, Γ is expressed as

$$\Gamma=\frac{\left|\int E^*(x,y,z=d)\cdot E(x,y,z=0)\right|^2}{|E(x,y,z=d)|^2\cdot|E(x,y,z=0)|^2} \tag{5}$$

where the integral is taken over the aperture of the receiving optics. The analysis here assumes a matrix-type $M\times N$ free-space MEMS optical switch, shown in Fig. 1, as an example. The algorithm can also be applied to general beam-steering free-space optical interconnection. The propagation distance d of the optical beam is determined by the pitch between the micromirrors. In our current designs, the pitch p and the mirror radius R obey the approximate geometrical relation

$$p=3R+800(\mu\text{m}). \tag{6}$$

For the following simulations, it is assumed that the distance from the emitting/receiving plane to the nearest mirror is $p/2$. The mirror radius R is used as a variable for the simulations, while the minimum Gaussian-beam width w_0 is related to R by $w_0=R/1.5$, so that most of the optical beam can be captured by the mirrors. The wavelength is assumed to be 1.55 μm, for comparison with experimental results. In fact, since these

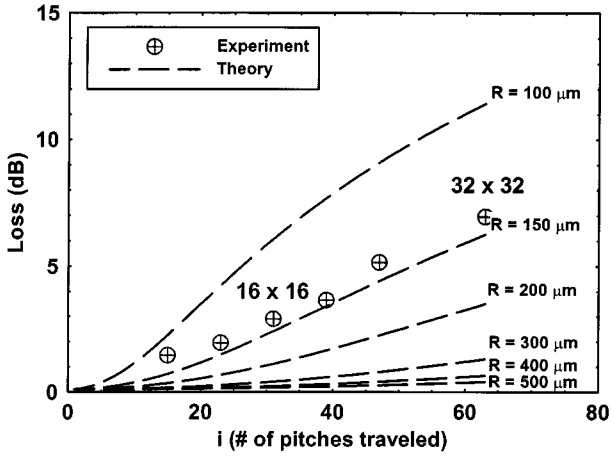

Fig. 3. Theoretical and experimental studies on loss versus propagation distance with various mirror radii for free-space MEMS optical switches.

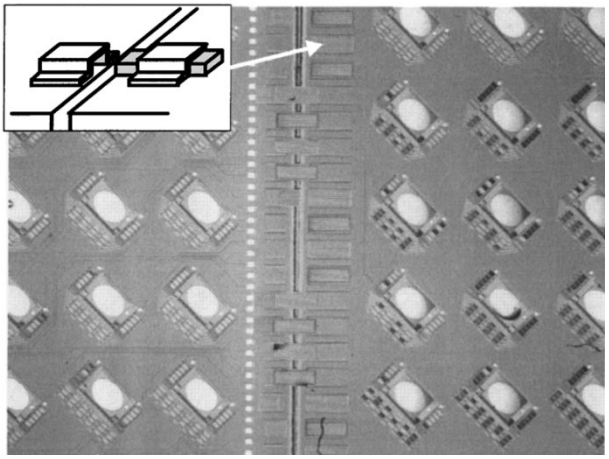

Fig. 4. Top-view of self-aligned polysilicon interchip bridging latches. Inset: latch-structure detail.

switches are envisioned as residing in an opaque network, light propagating through the OXC is likely be at 1.3 μm [11].

Fig. 3 plots calculated coupling loss versus number of mirror pitches traversed through a free-space micromachined cross connect. Coupling loss is seen to rise rapidly as the mirror and beam size decrease, suggesting that beam-divergence is the dominant factor in this region. However, it is an inherent feature of these devices that larger mirrors imply longer propagation paths. Therefore, the effect saturates for mirror radii $R > 400\,\mu$m.

To verify the simulation results, we measured coupling losses through a 16×16 cross connect built up from four basic 8×8 units. This was necessary due to foundry-imposed chip-size limits of 1 cm^2 [9]. In order to lock the four constituent chips together, we employed self-aligned interchip polysilicon bridging latches fabricated on the margins of each 8×8 chip. Fig. 4 depicts the polysilicon latches. Fig. 5 shows the assembled four-chip 16×16 cross connect. The switch-mirror radius is 150 μm. The latching structures were in fact used only for simulation purposes to provide first-order alignment. The angular alignment between the latched chips is not precise enough for optical-cross connect applications, and individual alignment between the input and output fiber

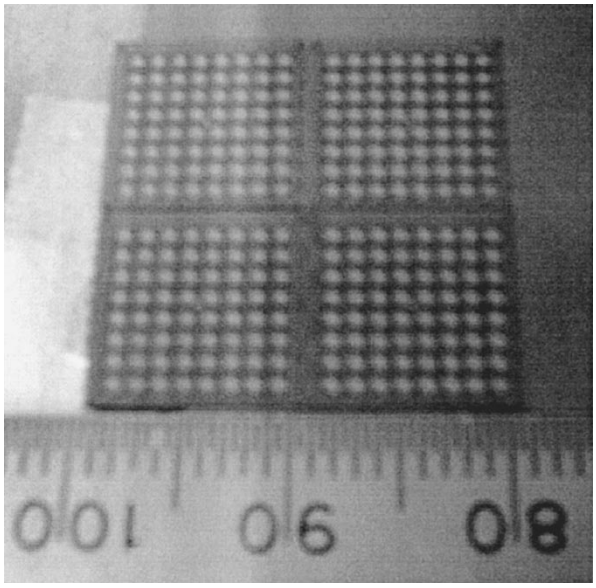

Fig. 5. Top view of a 16×16 cross-connect built-up from four latched 8×8 chips, each occupying 1 cm^2.

collimators are required. The four-chip latched cross connect provides a loss-measurement platform for switch size up to 16×16 when the fiber collimators are placed at the edge of the latched switch fabric. For larger cross connect sizes, measured losses were obtained by simply increasing the distance between the switch mirror and the fiber collimators, as required by the number of pitches that would need to be traversed. Measured coupling results for various cross connect sizes are shown in Fig. 3. Fiber-to-fiber losses of 2.9 dB were measured through the longest path of the 16×16 switch, while the measured loss for the simulated 32×32 switch is 6.9 dB. The experimental results are seen to agree well with the theoretical analysis.

III. Angular Dependence

A. Theory

The above results, while encouraging, capture only the properties of a cross connect that suffers divergence effects without penalty from optical misalignment. The dependence of coupling efficiency on angular misalignment of mirrors can be calculated by performing a coordinate-transformation on the Gaussian optical beam described above. We suppose that the angle of the micromirror is misaligned by $\theta/2$, resulting in an angular misalignment θ of the optical beam, as shown in Fig. 6. Furthermore, we define the distance from the mirror to the emitting plane and the transmitting plane as d_1 and d_2, respectively. The wave function of the optical beam after the micromirror now becomes

$$\begin{aligned} E(x', y, z') &= E_0 \left\{ \frac{w_0}{w(d_1+z')} \exp\left[-\frac{x'^2+y^2}{w^2(d_1+z')} \right] \right\} \\ &\quad \times \exp\left\{ -j \left[k(d_1+z') - \tan^{-1}\left(\frac{d_1+z'}{z_0} \right) \right] \right\} \\ &\quad \times \exp\left[-j \frac{k(x'^2+y^2)}{2R(d_1+z')} \right]. \end{aligned} \tag{7}$$

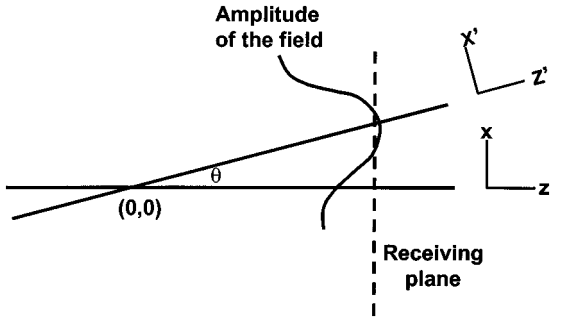

Fig. 6. Drawing depicting angular misalignment of the optical beam with respect to the receiving optics.

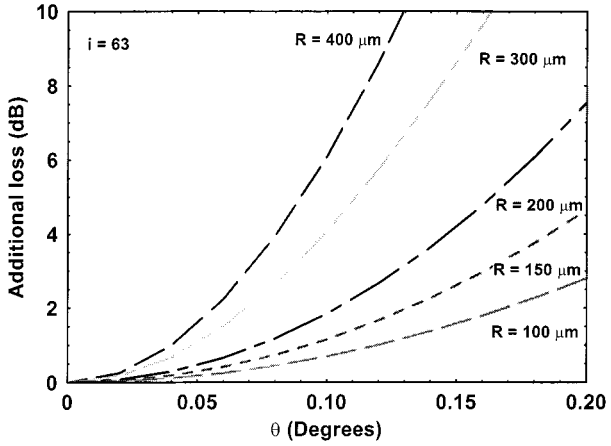

Fig. 7. Calculated additional loss due to angular misalignment for various mirror radii.

The coordinate $(x',\ z')$ is related to the original $(x,\ z)$ coordinate by

$$x' = x \cdot \cos(\theta) - z \cdot \sin(\theta)$$
$$z' = x \cdot \sin(\theta) + z \cdot \cos(\theta). \tag{8}$$

After substituting (8) into (7), the coupling efficiency can be obtained by calculating the normalized overlap integral of the optical beam wave function and the modal wave function of the receiving optics over the aperture of the receiving optics at the receiving plane ($z = d_2$):

$$\Gamma = \frac{\left|\int E^*(x', y, z') \cdot E(x, y, z = 0)\right|^2}{|E(x', y, z')|^2 \cdot |E(x, y, z = 0)|^2}. \tag{9}$$

Fig. 7 shows the simulation results for the maximum additional loss due to angular misalignment (i.e., the additional loss incurred by the longest path) in a 32×32 switch. It can be seen that larger optical beams, though less divergent, impose tighter angular tolerances. To verify this theoretical result, loss versus angular misalignment was measured using fiber collimators emitting a beam with $1/e$ half-width $w_0 = 160\ \mu$m. Between these collimators, a commercial mirror was mounted on a precision rotation stage with resolution of $1/60°$, and measured coupling loss was compared with calculations from (7) to (9). The results are shown in Fig. 8. The quality of agreement between the theoretical calculation and the experimental results

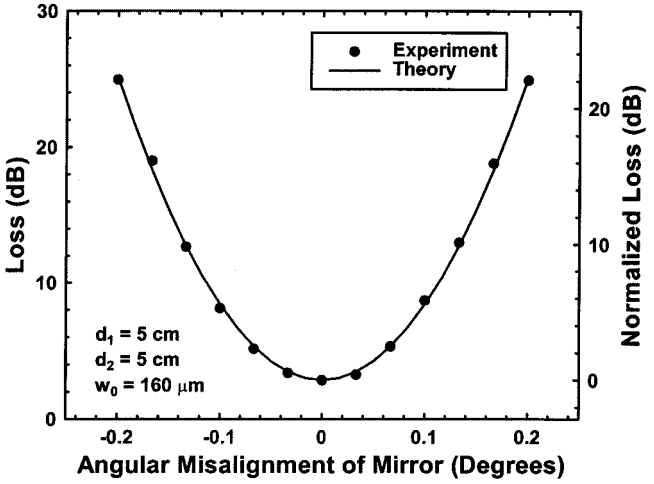

Fig. 8. Comparison between theoretical calculations and experimental results for loss versus angular misalignment.

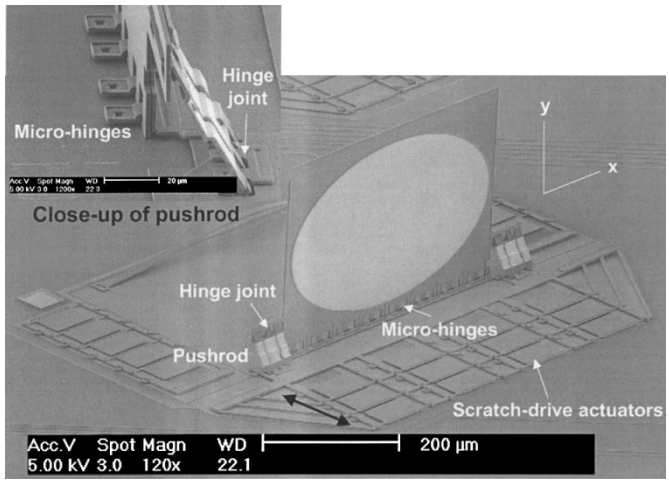

Fig. 9. SEM of the free-rotating hinged micromirror. Inset: pushrod detail.

suggests the validity of the coordinate-transformation computational approach described above.

B. Enhanced Micromechanical Registration Structures

The above results show that coupling efficiency is quite sensitive to angular alignment; thus, mechanisms for ensuring precise angular control of the micromirrors is crucial in free-space MEMS optical switches. The free-rotating micromirror in our approach (see Fig. 9) consists of a mirror frame anchored on the substrate by free-rotating hinges [12]. The mirror frame is connected to a translation stage via pushrods and hinge joints. Currently, scratch-drive actuators (SDA's) [13] are employed to move the translation stage. Both the inherent 0.75-μm clearance between the hinge pins and the hinge staples of the mechanism and the uncertainty in the moving distance of the micro-actuators will cause the angular misalignment of the micromirror.

We have developed mechanical alignment-enhancement structures that register micromirror angular position independently in the two orthogonal axes—θ_x and θ_y (defined in Fig. 9). The angular uncertainty in θ_y is caused mainly by the clearance in the fixed microhinges. The mirror frame has a width of 450 μm. Therefore, the maximum mirror-angular

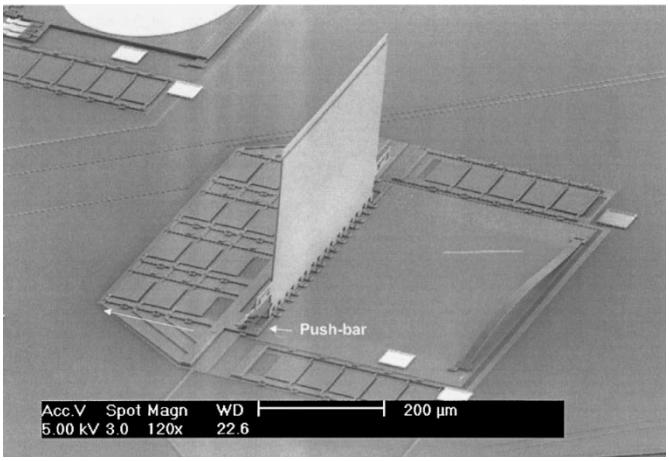

Fig. 10. SEM of a free-rotating hinged micromirror with push-bar structure for hinge-position enhancement.

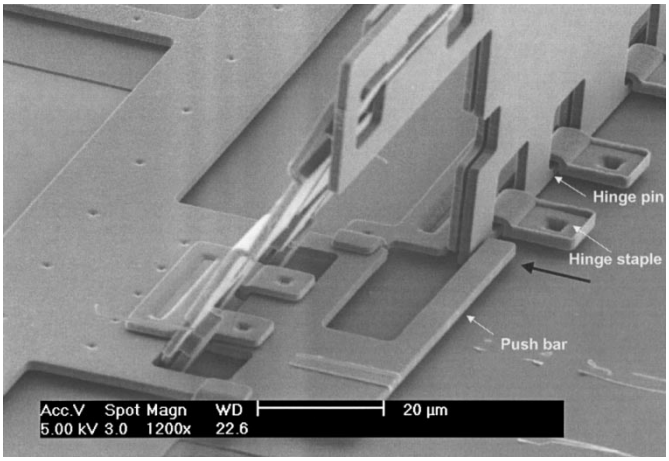

Fig. 11. Details of the microhinge and the push-bar.

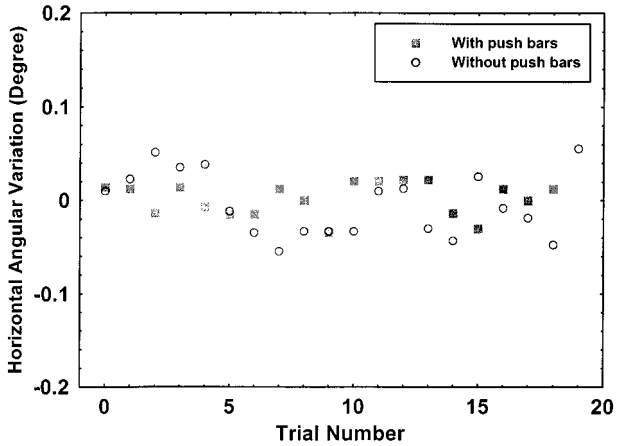

Fig. 12. Measured horizontal angular variation with and without the push-bars. The maximum variation is reduced from 0.056 to 0.034°.

variation will be $\tan^{-1}(1.5/450) = 0.19°$, which will cause substantial coupling loss. To register the hinge-pin position with precision surpassing the figure just mentioned, polysilicon push-bars are integrated with the translation stage, as shown in Fig. 10. As the translation stage moves forward, the push-bars on both sides of the mirror frame also move forward, and

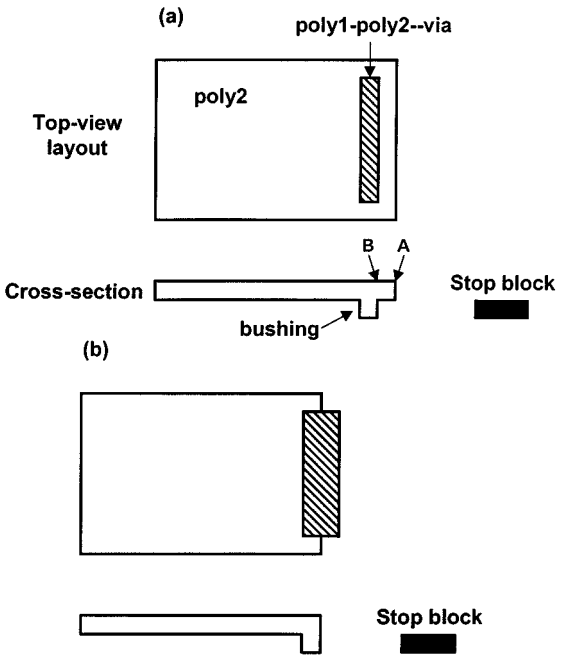

Fig. 13. (a) Conventional SDA design, where the stop position of the SDA is not clearly defined and (b) improved SDA design. The stop position of the SDA is clearly defined when the front-wall of the busing hits the stop block.

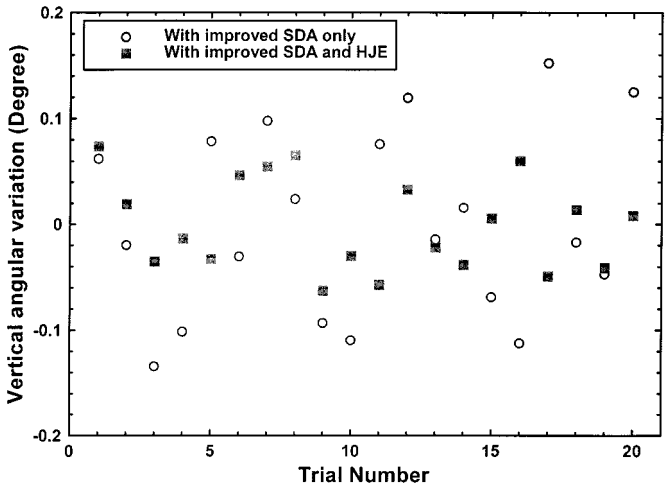

Fig. 14. Measured vertical angular variation. Circle: with improved SDA only. Square: with improved SDA and HJE (hinge-joint enhancement).

eventually push the hinge pins against the front-side of the hinge staples, thus eliminating the uncertainty in hinge-pin position. The detailed structure is shown in Fig. 11.

To measure the improvement in angular repeatability, a micromirror fabricated with integrated push-bars was actuated repeatedly, and the mirror-angle was obtained by measuring the position of the reflected optical beam spot at a screen 2-m away. The same measurement was then repeated for a micromirror without the push-bars. Fig. 12 shows the experimental results. With the push-bars, the maximum θ_y variation is reduced from 0.056 to 0.034°.

The vertical angular variation (θ_x) depends mainly on three variables: the clearance in the fixed microhinges, the clearance in the hinge-joints at the pushrod endpoints, and the moving distance of the translation stage. The first variable is improved by

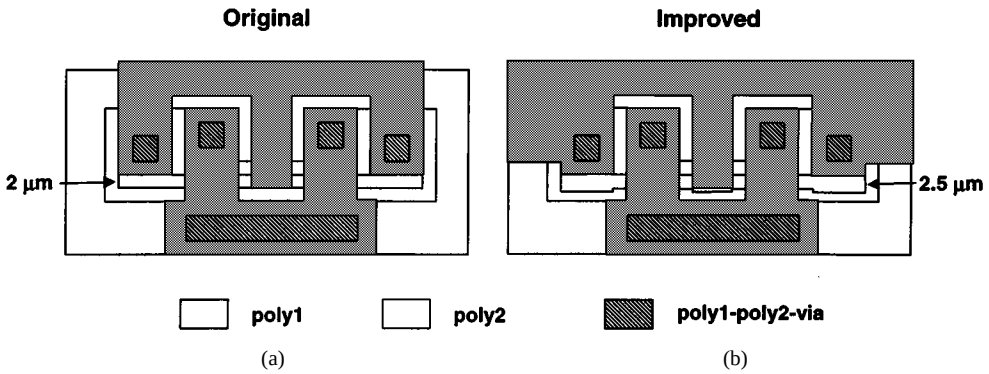

Fig. 15. (a) Layout of the original hinge joint. (b) Layout of the improved hinge joint. The hinge-pin position is restrained in the improved design.

the push-bar structures in Fig. 11, as described earlier. Nevertheless, without further improvement in the other two variables, a vertical angular variation greater than 1° can be easily observed. We propose two improvement schemes for the other two variables. They will be described in the following separately.

In the current designs where SDA's are employed as microactuators, the moving distance of the translation stage is mainly determined by the traveling distance of the SDA's. In conventional SDA design where fabrication tolerance is considered, the bushing of the SDA is located at a position 2 μm from the advancing edge of the SDA [see Fig. 13(a)]. The SDA travels until it hits the stop block on the substrate. The most reliable way to make a stop block with vertical side walls and without affecting the flatness of the underlying silicon nitride layer is by utilizing the poly-0 layer in the MUMPS process, which has a thickness of ~ 0.5 μm. The bushing is defined by the poly-2 layer atop the poly1–poly2-via in MUMPS process, which has a nominal height of 0.75 μm. Since these two heights are comparable, and there are both fabrication uncertainties and height variations of the SDA during actuation [13], the position where the SDA comes to rest against the stop block varies. Experimentally, various positions between A and B in Fig. 13(a) have been observed.

In order to eliminate this uncertainty, an extended poly1–poly2-via pattern is designed, as shown in Fig. 13(b). This results in a real "L"-shaped SDA, such that the SDA always stops when the front of the bushing hits the block. To measure the improvement in angular precision, a micromirror with this structure was actuated repeatedly, and the angular variation was plotted as circular data points in Fig. 14. The angular precision is improved from $\sim 1°$ to $0.15°$ through this improved SDA design.

The third uncertainty in controlling the vertical angular precision is the clearance in the free-rotating hinge joints. An improved free-rotating hinge joint was designed and found to minimize this effect. Fig. 15 shows the layout designs for the original and the improved hinge joints. The translation stage is connected to the poly1 layer, which has a thickness of 2 μm. The clearance between the poly2 hinge staple and the substrate is 2.75 μm. In the original hinge joint, the hinge pin has a uniform width of 2 μm. During actuation, the poly2 pushrod attached to the hinge pin is allowed to rotate and slide freely in the 6-μm m slot on the poly1 translation plate. This motion causes the uncertainty in the position of the hinge pin, and therefore the angle of the pushrod and the micromirror.

In the improved design, the part of the hinge pin that is not covered by the poly2 hinge staple has a width of 2.5 μm, while the rest still remains 2 μm to preserve its flexibility. As the pushrod is rotated up, the hinge pin starts to touch the hinge staple when the mirror angle approaches 90° (pushrod angle $\sim 70°$). The pressure from the hinge staple presses the hinge pin down and backward, thus preventing it from sliding. With this hinge-joint enhancement (HJE) structure in addition to the improved SDA described earlier, the maximum angular variation is further reduced to $0.074°$, as shown in Fig. 14.

IV. Improving Micromirror Flatness

In free-space MEMS optical switches, any curvature of the micromirrors affects the coupling efficiency dramatically. Although concave micromirrors can be used as focusing mirrors, the focal length and its repeatability is not easy to control during fabrication. Furthermore, micromirrors at different positions will require different focal lengths, which increases manufacturing complexity. Therefore, it is preferable to fabricate flat micromirrors with radius of curvature as large as possible. For the first-generation mirrors that were previously fabricated, the default gold layer in MUMPS process was employed for the reflecting mirror surface. This gold layer, with a thickness of 5000 Å, was directly deposited on the 1.5-μm-thick poly2 layer. The resulting thick gold-on-polysilicon slabs [Fig. 16(a)] exhibited curvature due to the internal stress between the thick gold coatings and the polysilicon layer. Fig. 17(a) shows a profilometer interferogram for one such mirror. The mirror surface is concave with a radius of curvature equal to 11.77 mm.

To solve this problem, we have employed the thick mirror structure of Fig. 16(b). A phosphosilicate glass (PSG) core is sandwiched between the 2-μm-thick poly1 and the 1.5-μm-thick poly2 layers, thus protecting it from the release etchant used in surface-micromachining. While this does not eliminate curvature entirely, it increases the radius of curvature to 16.12 mm [Fig. 17(b)]. Further improvement is achieved by depositing a thin layer of gold on the enhanced multilayer slab in Fig. 16(b) after the device is fabricated, without using the metallization of the MUMPS process itself. Fig. 17(c) shows the surface profile and the interferogram with a 500-Å gold

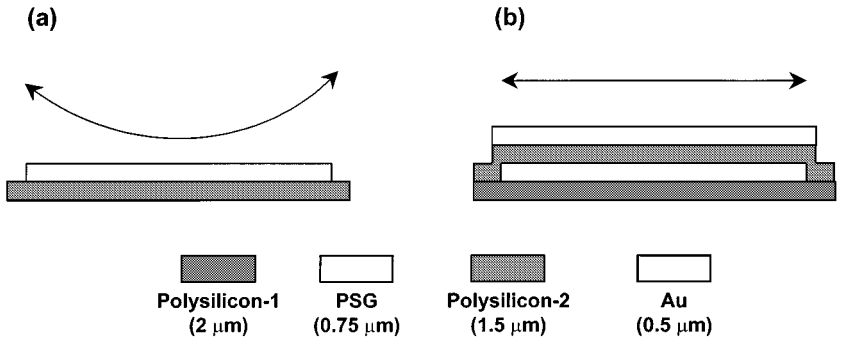

Fig. 16. Mirror-slab cross sections: (a) single-layer mirror slab and (b) improved structure achieving reduced mirror curvature via a phosphosilicate glass (PSG)-in-polysilicon sandwich.

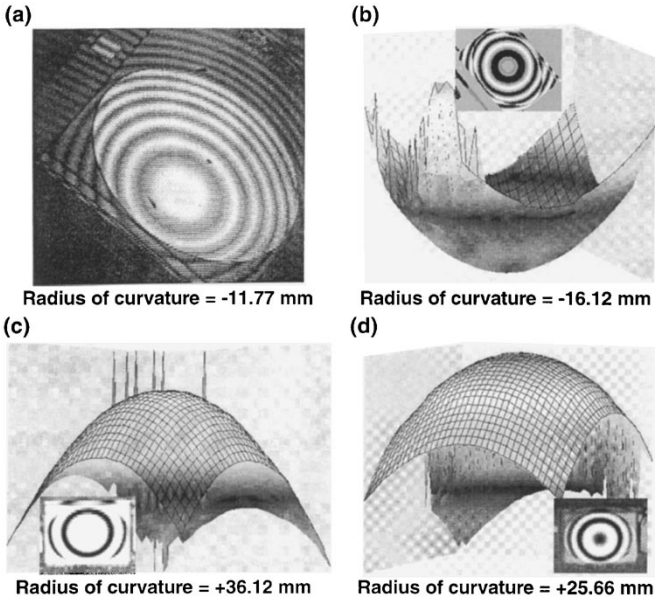

Fig. 17. Interferograms and surface profiles of micromirrors with: (a) single-layer with 5000-Å gold coating, (b) multilayer with 5000-Å gold coating, (c) multilayer with 500-Å gold coating, and (d) multilayer with 300-Å gold coating.

coating. The radius of curvature is increased to 36.12 mm. What is worth noting, however, is that the mirror-surface profile also changes from concave to convex. This suggests an optimum gold-layer thickness between 5000 and 500-Å, which can balance the material stress and achieve a nearly flat mirror. The surface-profile measurement of a thinner gold coating (300 Å), shown in Fig. 17(d), with smaller radius of curvature (25.66 mm) supports this conclusion. Using the thermal expansion coefficient of the current materials and assuming these materials are extremely flexible, the temperature dependence of the radius-of-curvature r is found to be $r = 358 \cdot (\Delta T)^{-1}$ (mm), where ΔT is measured in °C. To improve this, different materials should be employed. The reflectivity of both 5000- and 500-Å gold coating is 97% of a commercial gold mirror. The 300-Å gold-coated mirror has only 52% reflectivity. This structure is therefore expected to yield mirrors that are nominally flat, with reflectivity >97%, for a gold thickness in the bracketed region between 500 and 5000 Å.

V. Summary

We have theoretically analyzed the expandability of free-space MEMS optical switches by computing optical coupling efficiency using Gaussian-beam representations that are independent of the particular coupling optics employed. By incorporating a coordinate-transformation into the Gaussian-beam description, without approximation, we have also computed the effects of micromirror angular misalignment. The theoretical models were found to agree well with experimental measurements. Having thus characterized the importance of angular alignment in these systems, we have designed and demonstrated integrated mechanical structures that substantially enhance the angular repeatability of the micromirrors beyond limits that were observed in simple, first-generation devices. The measurement results show that angular precision better than 0.1° can be achieved. Finally, various material-layer structures have been investigated to improve the flatness of the mirror surfaces. The results show that it is possible to obtain nearly flat mirrors with good optical quality. In view of the swift progress thus seen in mitigating these problems, it appears that the main challenges for free-space MEMS optical-switching technology are posed not by fundamental physical limits in reaching the required optical performance, but by practical reliability and packaging concerns.

Acknowledgment

The authors would like to thank JDS Fitel, Inc., for their collaboration on packaging issues.

References

[1] S.-S. Lee, L.-S. Huang, C.-J. Kim, and M. C. Wu, "Free-space fiber-optic switches based on MEMS vertical torsion mirrors," *J. Lightwave Technol.*, vol. 17, pp. 7–13, 1999.

[2] C. Marxer and N. F. de Rooij, "Micro-opto-mechanical 2×2 switch for single-mode fibers based on plasma-etched silicon mirror and electrostatic actuation," *J. Lightwave Technol.*, vol. 17, pp. 2–6, 1999.

[3] H. Toshiyoshi and H. Fujita, "Electrostatic micro torsion mirrors for an optical switch matrix," *J. Microelectromechan. Syst.*, vol. 5, pp. 231–237, 1996.

[4] L. Y. Lin, E. L. Goldstein, and R. W. Tkach, "Free-space micromachined optical switches for optical networking," *IEEE J. Select. Topics Quantum Electron.: Special Issue on Microoptoelectromechanical Systems (MOEMS)*, vol. 5, pp. 4–9, 1999.

[5] R. T. Chen, H. Nguyen, and M. C. Wu, "A low voltage micromachined optical switch by stress-induced bending," in *Proc. 12th IEEE Int. Conf. Micro Electro Mechanical Syst.*, Orlando, FL, 1999.
[6] B. Behin, K. Y. Lau, and R. S. Muller, "Magnetically Actuated micromirrors for fiber-optic switching," in *Proc. Solid-State Sensor and Actuator Workshop*, Hilton Head Island, SC, 1998.
[7] H. Laor, "MEMS mirrors application in optical cross-connects," in *Proc. IEEE LEOS Summer Topical Meetings: Optical MEMS*, Monterey, CA, 1998.
[8] C. Marxer, M.-A. Grètillat, N. F. de Rooij, R. Bättig, O. Anthamatten, B. Valk, and P. Vogel, "Reliability considerations for electrostatic polysilicon actuators using as an example the REMO component," *Sensors Actuators A*, vol. 61, pp. 449–454, 1997.
[9] Cronos Integrated Microsystems Inc.http://www.memsrs.com.
[10] J. T. Verdeyen, *Laser Electronics*, 2nd ed. Englewood Cliffs, NJ: Prentice-Hall, 1989.
[11] E. L. Goldstein, J. A. Nagel, J. L. Strand, and R. W. Tkach, "Multiwavelength opaque optical-crossconnect networks," *J. Lightwave Technol.*, vol. 17, pp. 92–95, 1998.
[12] K. S. J. Pister, M. W. Judy, S. R. Burgett, and R. S. Fearing, "Microfabricated hinges," *Sensors Actuators A*, vol. 33, pp. 249–256, 1992.
[13] T. Akiyama and H. Fujita, "A quantitative analysis of scratch drive actuator using buckling motion," in *Proc. IEEE Workshop on Micro Electro Mechanical Systems*, Amsterdam, The Netherlands, 1995.

Lih-Yuan Lin (S'93–M'96) received the M.S. and Ph.D. degrees in electrical engineering from the University of California at Los Angeles (UCLA) in 1993 and 1996, respectively.

In 1996, she joined the Lightwave Networks Research Department of AT&T Labs-Research, Red Bank, NJ, as a Senior Technical Staff Member, where she worked on micromachined technologies for optical switching and lightwave components, as well as WDM network architectures. She is currently with Tellium, Inc., Oceanport, NJ. She has more than 100 publications in the areas of optical MEMS, high-speed photodetectors, and network architectures. She holds four U.S. patents and has five more pending.

Dr. Lin is a member of the Optical Society of America (OSA) and Photonics Society of Chinese-Americans. She has served on the Technical Program Committee of 1998 IEEE LEOS Summer Topical Meeting on Optical MEMS, Third International Conference on Micro Opto Electro Mechanical Systems (MOEMS'99), and as the organizer for 1999 OSA Annual Meeting on MEMS for Photonics. She is now one of the steering committee members of the International Optical MEMS Conference.

Evan L. Goldstein (S'84–M'89) was born in Seattle, WA, in 1952. He received the B.A. degree in philosophy from Antioch College, Yellow Springs, OH, in 1975, and the M.A. and M.Phil. degrees in philosophy from Columbia University, New York, NY, in 1977 and 1981, respectively. He also received the B.S., M.S., and Ph.D. degrees from Columbia University in 1985, 1986, and 1989.

He taught undergraduate courses at Columbia University in philosophy, history of science, and intellectual history during the late 1970's and later switched to electrical engineering. Since joining Bellcore in 1986, and subsequently moving to AT&T Laboratories, he has done research on various aspects of lightwave systems, focusing on optical-fiber amplifiers, on lightwave system-performance, and on architectural issues in WDM networks. He was a Principal Technical Staff Member in the Lightwave Networks Research Department at AT&T Labs, Red Bank, NJ. He is currently with Tellium, Inc., Oceanport, NJ.

Robert W. Tkach (M'84–SM'98) was born in Lorain, OH, in 1954. He received the Ph.D. degree in physics from Cornell University, Ithaca, NY, in 1982.

From 1982 to 1984, he was a Postdoctoral Research Associate at Cornell University. In 1984, he joined the staff of AT&T Bell Laboratories, Red Bank, NJ, investigating various aspects of lightwave communications systems including semiconductor lasers, optical networks, and nonlinear optical effects in fibers. In recent years, his research activities have focused on the demonstration of ultrahigh-capacity transmission systems based on wavelength-division multiplexing, and on the application of optical networking in long-haul transport networks. He is currently Head of the Lightwave Networks Research Department at AT&T Labs.

Dr. Tkach is an AT&T Fellow and a Fellow of the Optical Society of America (OSA).